Supplementary materials for "Projection-pursuit Bayesian regression for symmetric matrix predictors"

Below we provide supplementary results for Sections 3 and 4 in our paper "Projection-pursuit Bayesian regression for symmetric matrix predictors"

1 Simulation

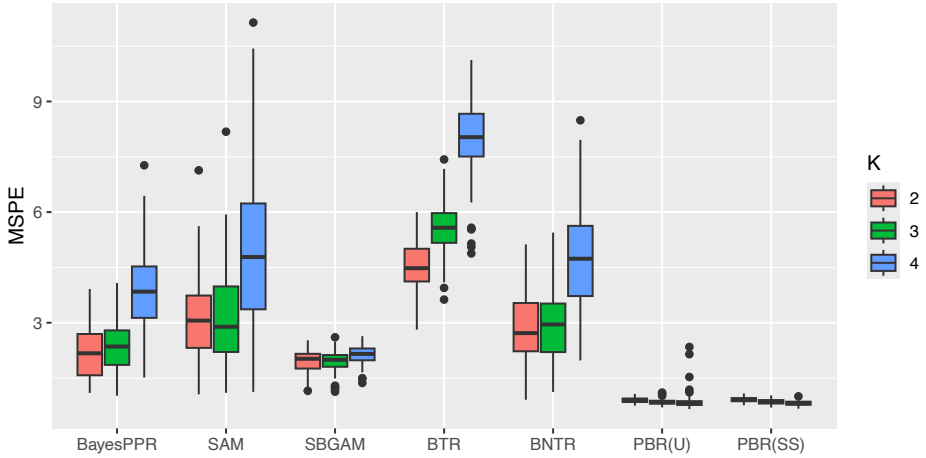

Fig. 1: Mean-squared prediction error (MSPE) on training sets for settings with $p = 15$ and $K \in \{2, 3, 4\}$ from 100 runs of the experiment in the "correctly specified" scenario.

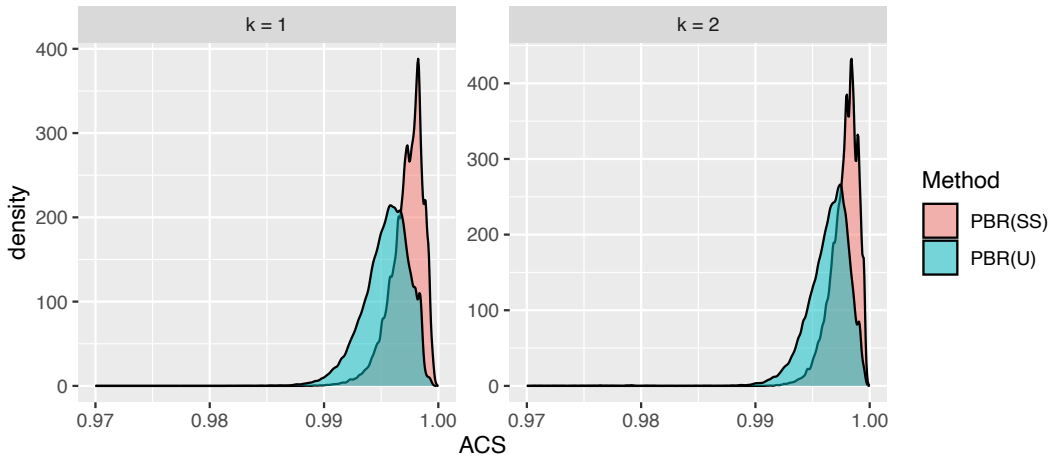

Fig. 2: Density of the absolute cosine similarity (ACS) of $\boldsymbol{\gamma}_k$'s for the $p = 15$, $K = 2$ setting from 100 runs of the experiment.

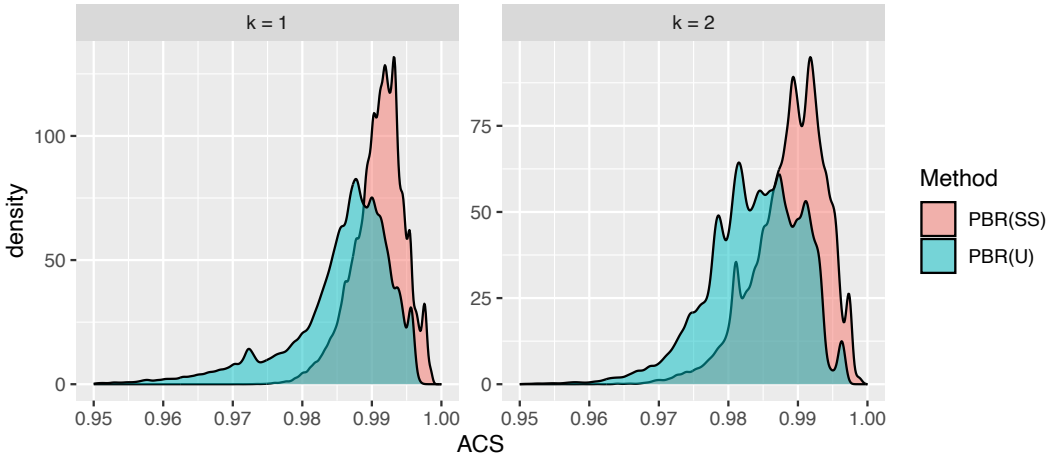

Fig. 3: Density of the absolute cosine similarity (ACS) of $\boldsymbol{\gamma}_k$'s for the $p = 25$, $K = 2$ setting from 100 runs of the experiment.

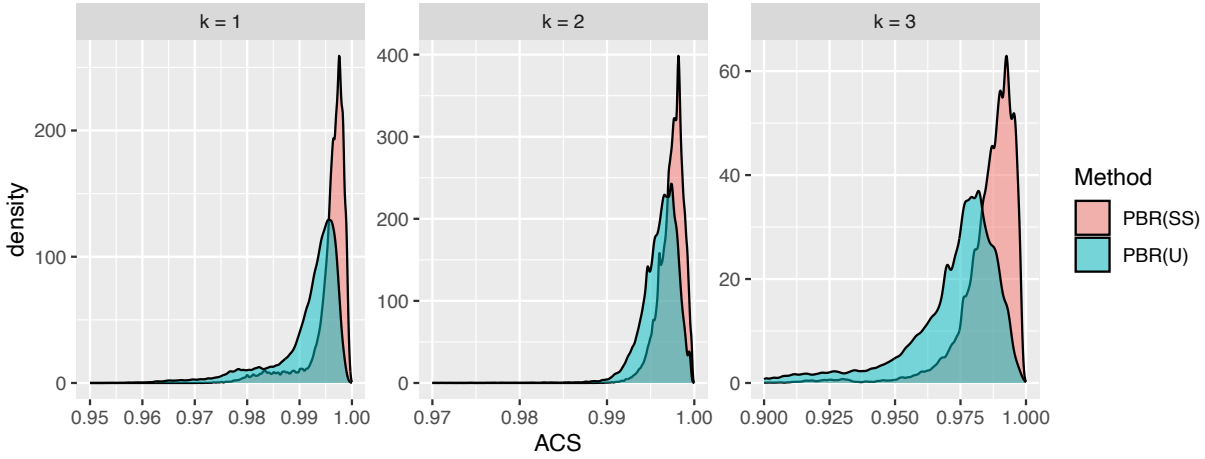

Fig. 4: Density of the absolute cosine similarity (ACS) of $\boldsymbol{\gamma}_k$'s for the $p = 15$, $K = 3$ setting from 100 runs of the experiment.

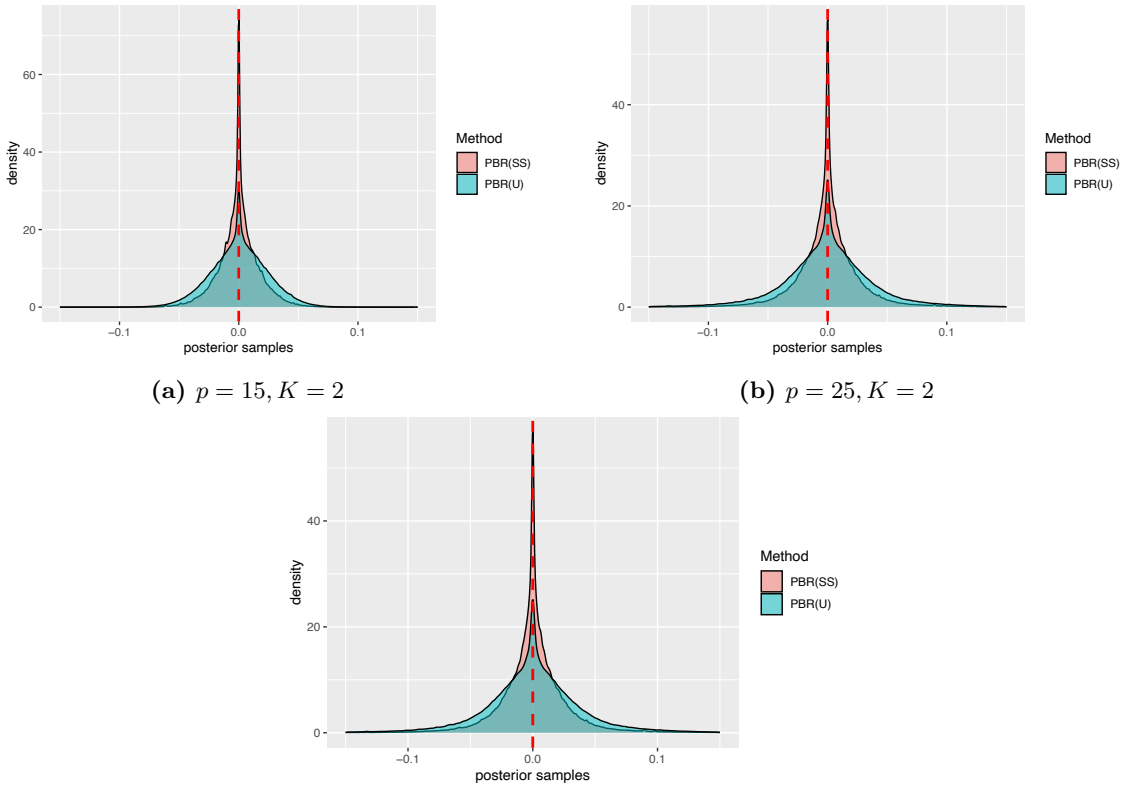

(a) $p = 15, K = 2$

(b) $p = 25, K = 2$

(c) $p = 15, K = 3$

Fig. 5: Density of posterior samples for the true zero elements of $\boldsymbol{\gamma}_k$'s for three settings: $p = 15, K = 2$ (top left panel), $p = 25, K = 2$ (top right panel), and $p = 15, K = 3$ (bottom panel), generated with samples aggregated for $k \in \{1, \ldots, K\}$ from 100 runs of the experiment.

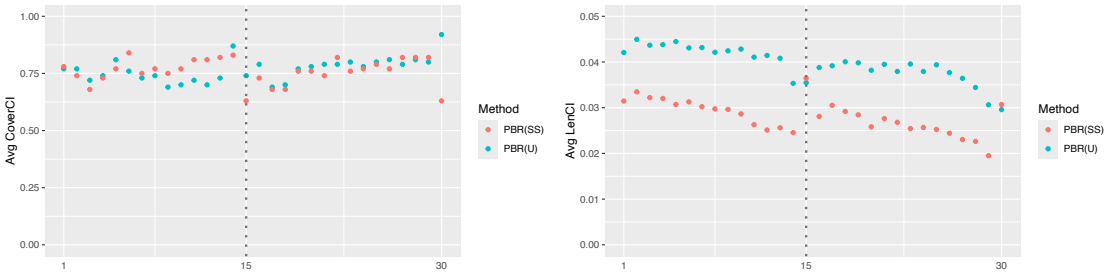

(a) CoverCI **(b)** LenCI

Fig. 6: CoverCI and LenCI for the $p = 15$ and $K = 2$ setting for each element of $\boldsymbol{\gamma}_k$'s, averaged across 100 runs of the experiment.

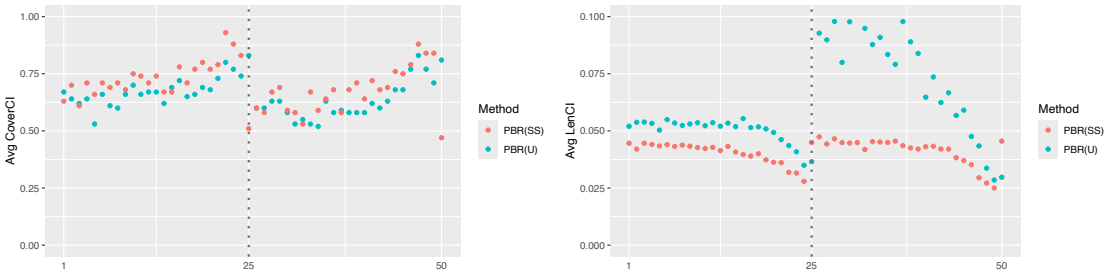

(a) CoverCI **(b)** LenCI

Fig. 7: CoverCI and LenCI for the $p = 25$ and $K = 2$ setting for each element of $\boldsymbol{\gamma}_k$'s, averaged across 100 runs of the experiment.

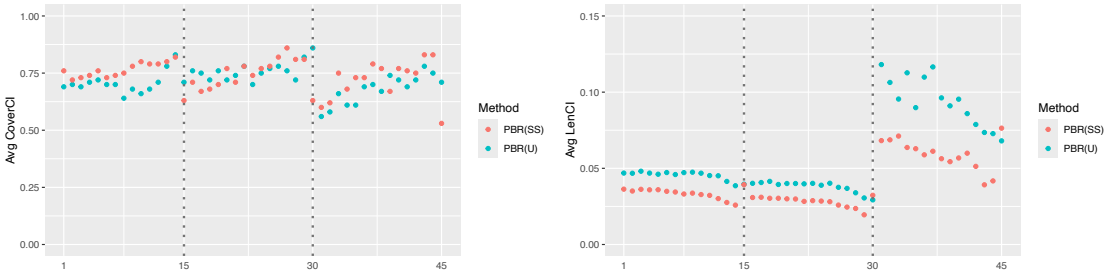

(a) CoverCI **(b)** LenCI

Fig. 8: CoverCI and LenCI for the $p = 15$ and $K = 3$ setting for each element of $\boldsymbol{\gamma}_k$'s, averaged across 100 runs of the experiment.

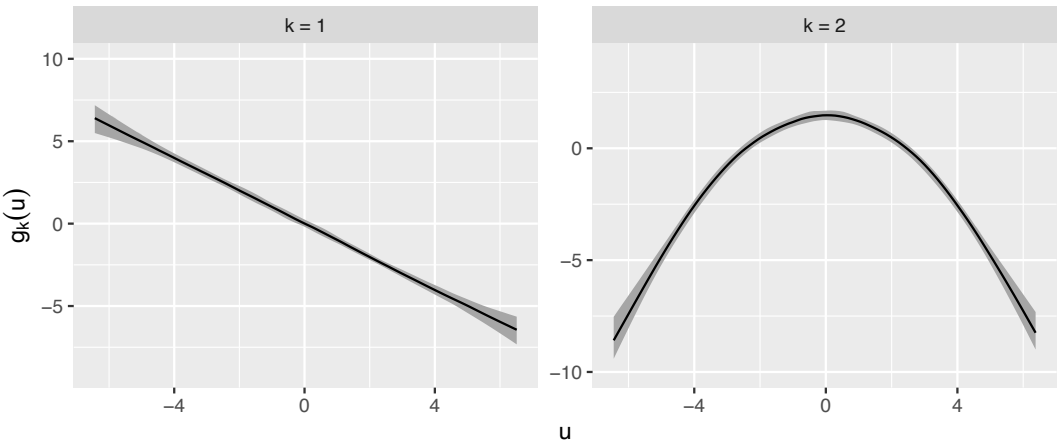

(a) PBR(U)

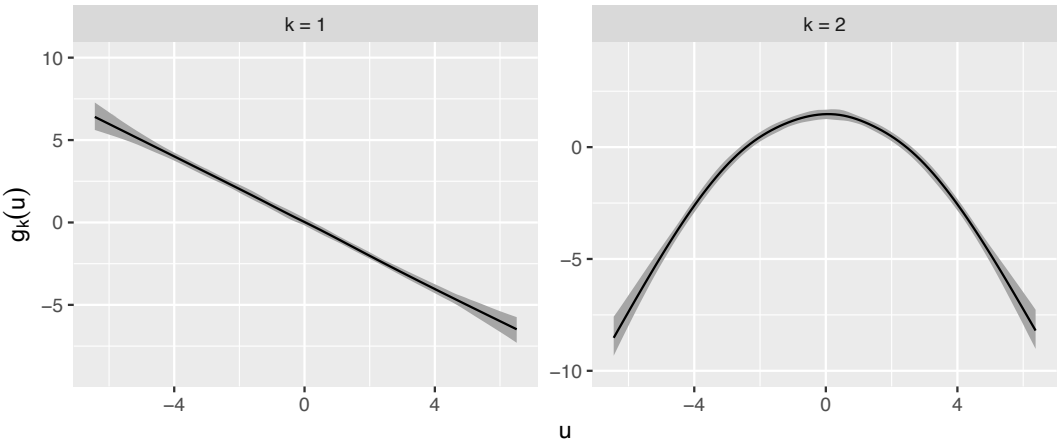

(b) PBR(SS)

Fig. 9: Median and 80% credible intervals for the posterior samples of ridge functions (g_k's) generated by **PBR(U)** and **PBR(SS)** for the $p = 15$ and $K = 2$ setting aggregated across 100 runs of the experiment.

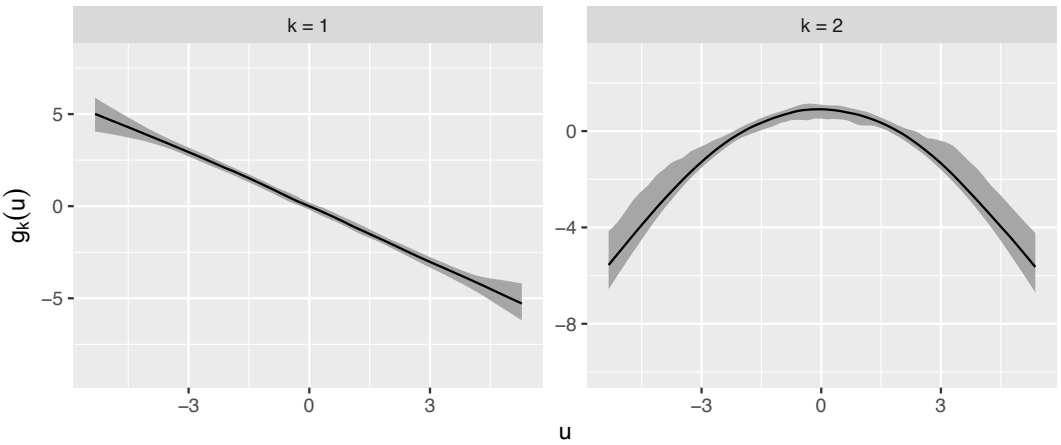

(a) PBR(U)

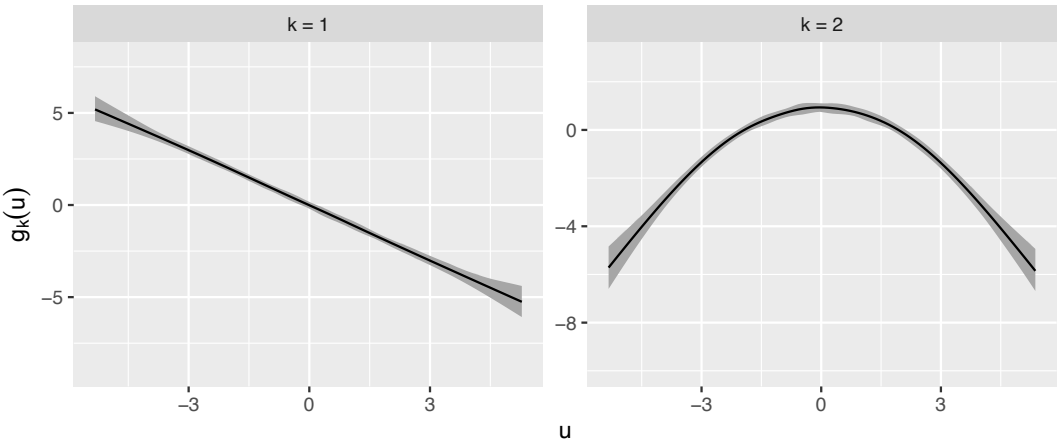

(b) PBR(SS)

Fig. 10: Median and 80% credible intervals for the posterior samples of ridge functions (g_k's) generated by **PBR(U)** and **PBR(SS)** for the $p = 25$ and $K = 2$ setting aggregated across 100 runs of the experiment.

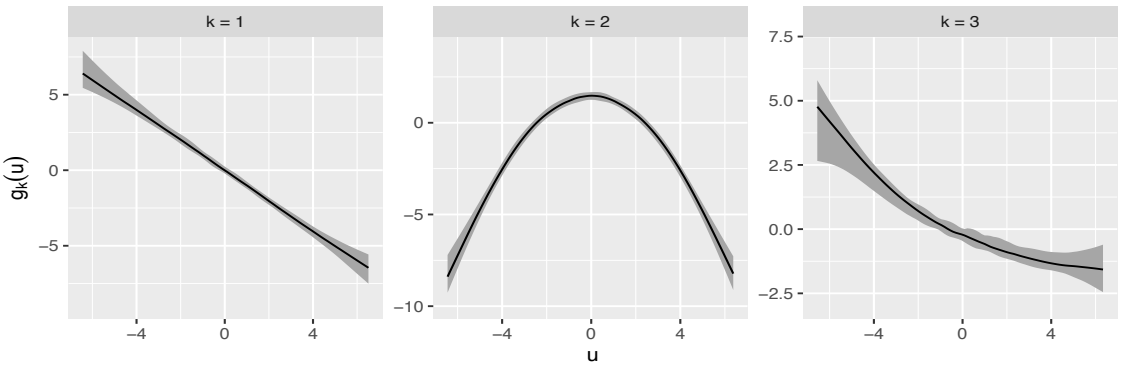

(a) PBR(U)

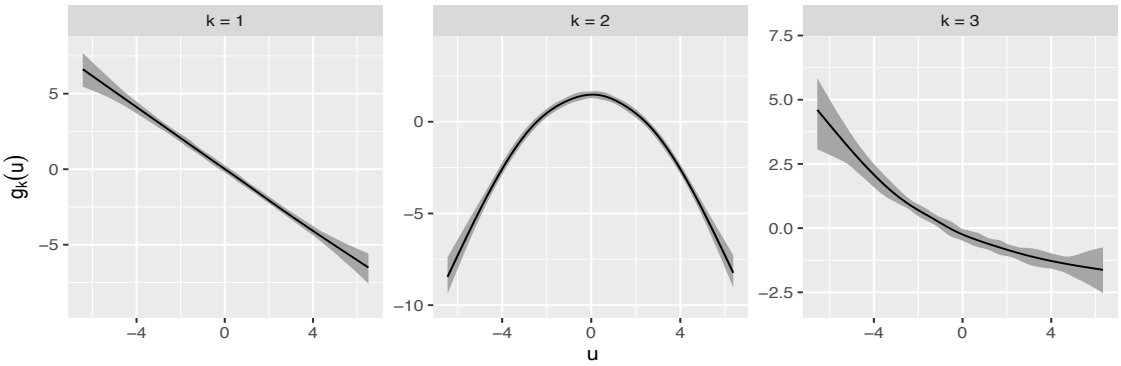

(b) PBR(SS)

Fig. 11: Median and 80% credible intervals for the posterior samples of ridge functions (g_k's) generated by **PBR(U)** and **PBR(SS)** for the $p = 15$ and $K = 3$ setting aggregated across 100 runs of the experiment.

2 Application

Below, we present the results using the connectivity of $p = 25$ brain regions to predict age-adjusted early childhood composite score (CogEarlyComp_AgeAdj) from the Human Connetome Project (HCP). The following results for **PBR** were obtained with $K = 3$, which yields better predictive performance compared to $K = 2$ presented for the $p = 15$ case in the manuscript.

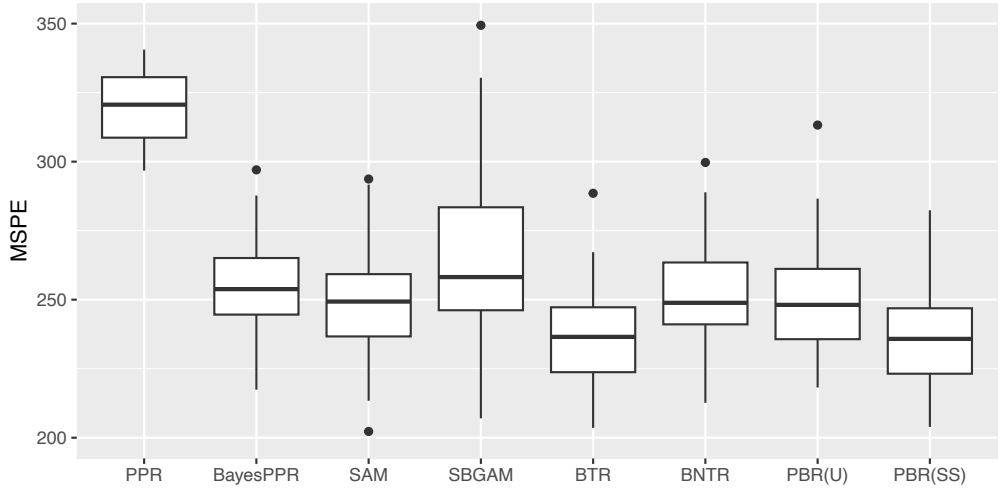

Fig. 12: Mean-squared prediction error (MSPE) on test sets obtained from 50 random data splits.

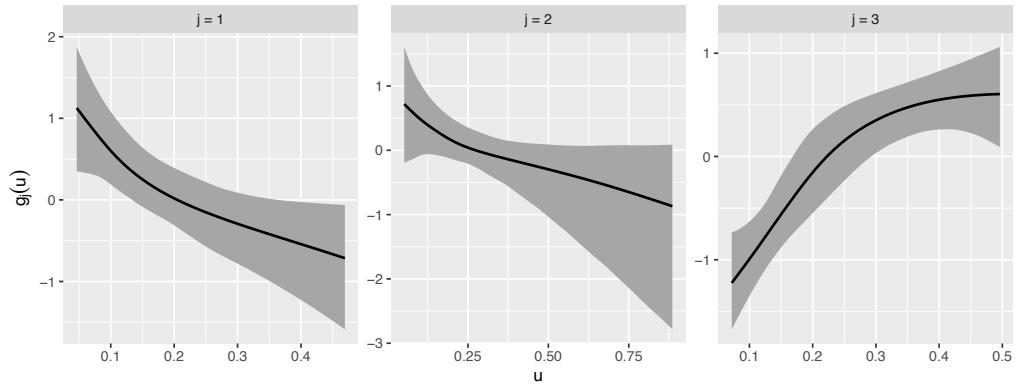

Fig. 13: Median and 80% credible intervals for the posterior samples of ridge functions (g_k's) generated by **PBR(SS)** aggregated across 50 runs, each with a random data split.

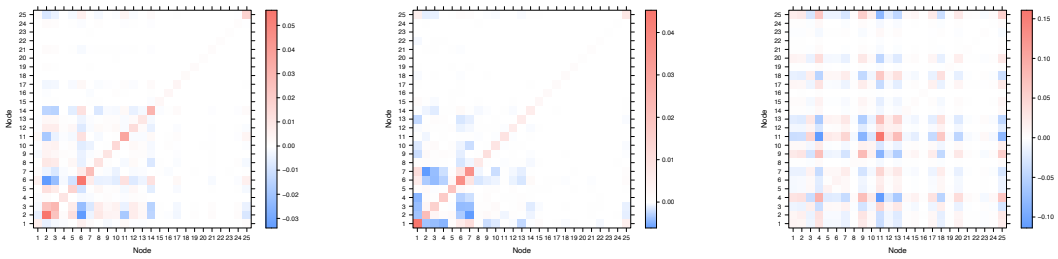

(a) $\gamma_1\gamma_1^T$ **(b)** $\gamma_2\gamma_2^T$ **(c)** $\gamma_3\gamma_3^T$

Fig. 14: Median of the posterior samples of $\gamma_k\gamma_k^T$'s for $p = 25$ generated by **PBR(SS)** aggregated across 50 runs, each with a random data split. White color indicates a value of zero.

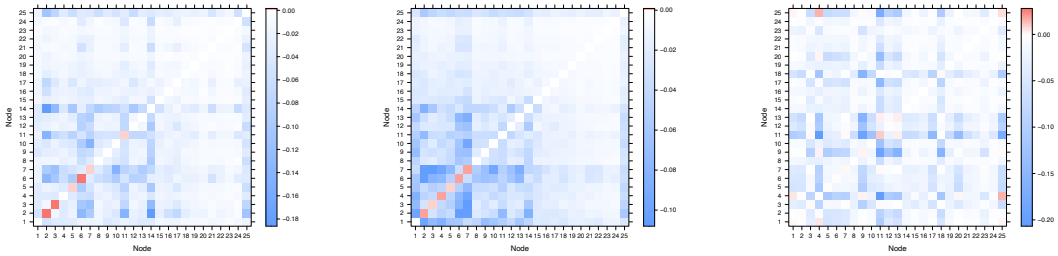

(a) $\gamma_1\gamma_1^T$ **(b)** $\gamma_2\gamma_2^T$ **(c)** $\gamma_3\gamma_3^T$

Fig. 15: 10% quantile of the posterior samples of $\gamma_k\gamma_k^T$'s for $p = 25$ generated by **PBR(SS)** and aggregated across 50 runs, each with a random data split. White color indicates a value of zero.

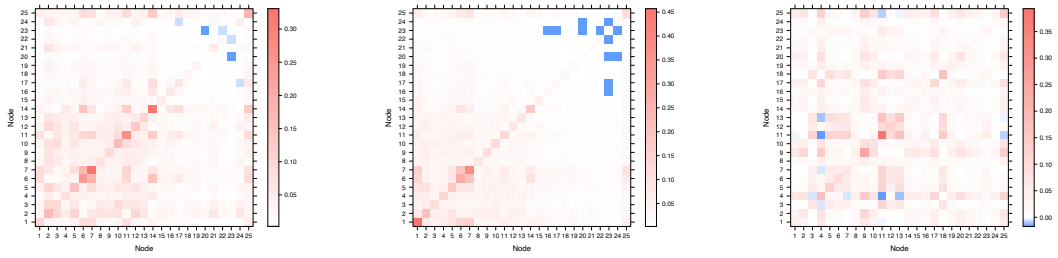

(a) $\gamma_1\gamma_1^T$ **(b)** $\gamma_2\gamma_2^T$ **(c)** $\gamma_3\gamma_3^T$

Fig. 16: 90% quantile of the posterior samples of $\gamma_k\gamma_k^T$'s for $p = 25$ generated by **PBR(SS)** and aggregated across 50 runs, each with a random data split. White color indicates a value of zero.

For the case presented in the manuscript, using the connectivity of $p = 15$ brain regions for inference and prediction, we present the 10% and 90% quantiles of $\gamma_1\gamma_1^T$ and $\gamma_2\gamma_2^T$.

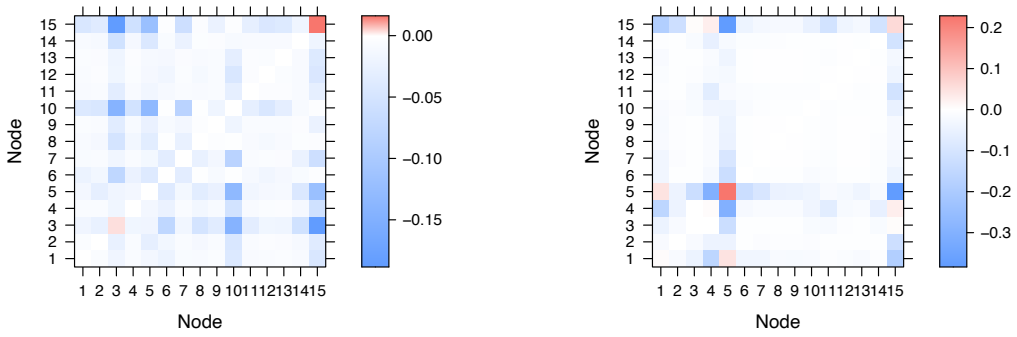

(a) $\gamma_1\gamma_1^T$ **(b)** $\gamma_2\gamma_2^T$

Fig. 17: 10% quantile of the posterior samples of $\gamma_k\gamma_k^T$'s for $p = 15$ generated by **PBR(SS)** and aggregated across 50 runs, each with a random data split. White color indicates a value of zero.

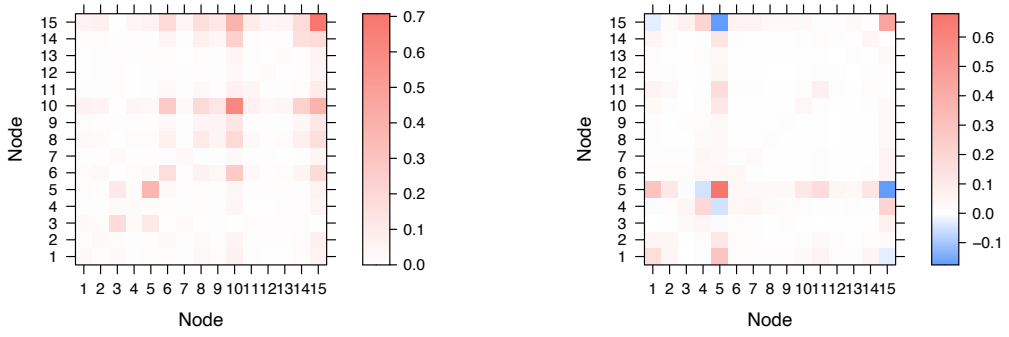

(a) $\gamma_1\gamma_1^T$ **(b)** $\gamma_2\gamma_2^T$

Fig. 18: 90% quantile of the posterior samples of $\gamma_k\gamma_k^T$'s for $p = 15$ generated by **PBR(SS)** and aggregated across 50 runs, each with a random data split. White color indicates a value of zero.